JOURNAL OF VIROLOGY, May 2005, p. 5799–5811 Vol. 79, No. 9
0022-538X/05/$08.00+0 doi:10.1128/JVI.79.9.5799–5811.2005

Tumorigenic Poxviruses Up-Regulate Intracellular Superoxide To Inhibit Apoptosis and Promote Cell Proliferation

Melissa L. T. Teoh,[1] Patricia V. Turner,[2] and David H. Evans[1]*

Department of Medical Microbiology & Immunology, Faculty of Medicine and Dentistry, The University of Alberta, Edmonton, Alberta, T6G 2H7 Canada,[1] and Department of Pathobiology, Ontario Veterinary College, The University of Guelph, Guelph, Ontario, N1G 2W1 Canada[2]

Received 27 October 2004/Accepted 3 December 2004

Tumorigenic leporipoxviruses encode catalytically inactive homologs of cellular Cu-Zn superoxide dismutase (SOD1). The function of the orthologous myxoma virus M131R and Shope fibroma virus S131R gene products is uncertain, but they inhibit SOD1 activity by a process linked to binding its copper chaperone. Using a superoxide-sensitive dye (hydroethidine), we observed that virus infection increased intracellular superoxide levels in an M/S131R-dependent manner. To see whether this effect promotes infection, we deleted the Shope fibroma virus S131R gene and compared the clinical manifestations of wild-type and mutant virus infections in rabbits. S131RΔ virus produced significantly smaller fibroxanthosarcoma-like growths in vivo and, at a point where these growths were already receding, wild-type infections still showed extensive leukocyte infiltration, necrosis, and fibromatous cell proliferation. Coincidentally, whereas Jurkat cells are protected from mitochondria- and Fas-mediated apoptosis by wild-type myxoma virus in vitro, M131RΔ virus could not block Fas-initiated apoptosis as judged by DNA laddering, terminal deoxynucleotidyltransferase-mediated dUTP-fluorescein nick end labeling, and caspase 3 cleavage assays. These data suggest that tumorigenic poxviruses can modulate intracellular redox status to their advantage to stimulate infected cell growth and inhibit programmed cell death.

Redox phenomena serve a critical function in numerous biological and biochemical processes. Reactive oxygen species (ROS) are generated during normal cellular metabolism as well as by activated phagocytes in response to infection (15, 21, 27). Since the intracellular accumulation of toxicants like superoxide radical ($O_2\cdot^-$), hydrogen peroxide, and hydroxyl radical is undesirable, ROS levels are usually tightly limited by multiple cellular mechanisms. They are also closely regulated, because superoxide plays an important role as a secondary messenger in mediating inflammation, stimulating cell proliferation, and regulating apoptosis (reviewed in references 3, 4, and 28). This has led to the widely accepted premise that the regulation of redox homeostasis is important in determining when cells rest, proliferate, or die.

One of the key enzymes involved in maintaining this regulatory net is Cu-Zn superoxide dismutase 1 (SOD1), an enzyme that catalyzes the removal of superoxide radicals through their chemical dismutation (15, 16). Mutations in SOD1 have been causally linked to the familial form of human amyotrophic lateral sclerosis (34), but there have been many persistent reports that tumor cells also exhibit deficiencies in SOD1 activity along with elevated levels of $O_2\cdot^-$ and other ROS (e.g., references 6, 18, and 45). The significance of these observations is hard to judge, given the genetic diversity of transformed cells and the sometimes contradictory evidence (reviewed in reference 24). However, gene transfection methods have been used more recently to directly manipulate SOD1 activity in transformed cells, and this has been seen to alter the growth rate, tumor formation, and metastatic potential of these cells (14, 47, 58). These and other observations have led to the suggestion that increasing the concentration (or flux) of intracellular superoxide can promote tumor growth and survival. One of the most plausible mechanisms by which ROS can do this arises from the observation that superoxide (or its metabolite, H_2O_2) can stimulate the activity of mitogen-activated kinases. This can in turn promote cellular transformation, proliferation, and metastasis (3, 4).

Interestingly, many large DNA viruses encode SOD1 homologs, including baculoviruses and poxviruses. The first of the SOD1-like poxvirus genes to be discovered was the A45R gene encoded by the *Orthopoxvirus* vaccinia (1, 43), but sequencing later showed that leporipoxviruses encode similar genes which even more closely resemble cellular SOD1 and which have been designated M131R and S131R in myxoma virus (MYX) and Shope fibroma virus (SFV), respectively (9, 55). MYX and SFV are sometimes called tumorigenic poxviruses because they produce fibroxanthosarcoma-like tumor growths when infecting their natural hosts (New World hares). These growths are relatively benign in adult animals and regress over 3 to 4 weeks due to a combined humoral and cell-mediated immune response (37, 44). We have been using MYX and SFV to elucidate the biological function of these enigmatic genes.

M131R and S131R encode 96% identical, catalytically inactive, late proteins. They are nonessential proteins that are nevertheless packaged in large quantities in virus particles and promote a gradual reduction in SOD1 activity in virus-infected cells (9). These proteins cannot bind copper, which is essential for dismutase activity, but they have retained the zinc-binding properties of their cellular homolog and similarly form stable heterodimeric complexes with the cellular copper chaperone

* Corresponding author. Mailing address: Dept. Microbiology and Immunology, University of Alberta, 141 Medical Sciences Building, Edmonton, AB T6G 2H7, Canada. Phone: (780) 492-2308. Fax: (780) 492-7521. E-mail: devans@ualberta.ca.

for SOD1 (49). Copper chaperone for SOD1 (CCS) serves the essential purpose of cuprolating SOD1 (25, 35). These observations led us to hypothesize that M131R and S131R gene products are protein "decoys" which compete with SOD1 for CCS activity and thus deplete the copper supply to the cellular enzyme (49). In doing this, SFV and MYX (and possibly other poxviruses) may be exploiting the fact that CCS seems to serve a critical role in regulating SOD1 activity (12).

Studying what role these genes might play in virus pathogenesis requires a careful choice of animal model. MYX causes myxomatosis in European laboratory rabbits (*Oryctolagus cuniculus*), but the high mortality, rapid systemic spread, and profound immunodeficiency characteristic of myxomatosis are very different from the benign infections MYX causes in *Sylvilagus* hares. Perhaps consequentially we could not detect any obvious requirement for M131R gene function using this virulent disease model, beyond a slight delay in the appearance and spread of the primary lesion (9). In contrast, SFV naturally lacks several genes essential for MYX pathogenesis (8) and produces a disease in rabbits that more closely recapitulates the disease course seen in *Sylvilagus* hares. Using this infection model we show here that SFV mutant viruses lacking the S131R gene produce much smaller and faster-regressing tumors than does wild-type virus. S131R-deficient viruses are also unable to up-regulate superoxide levels or suppress Fas-mediated apoptotic induction like wild-type SFV. These studies illustrate a novel mechanism of viral pathogenesis, wherein tumorigenic poxviruses manipulate intracellular superoxide levels to promote infected cell growth and immune evasion, and may ultimately provide insights into the role ROS and redox status play in regulating other forms of tumor growth and metastasis.

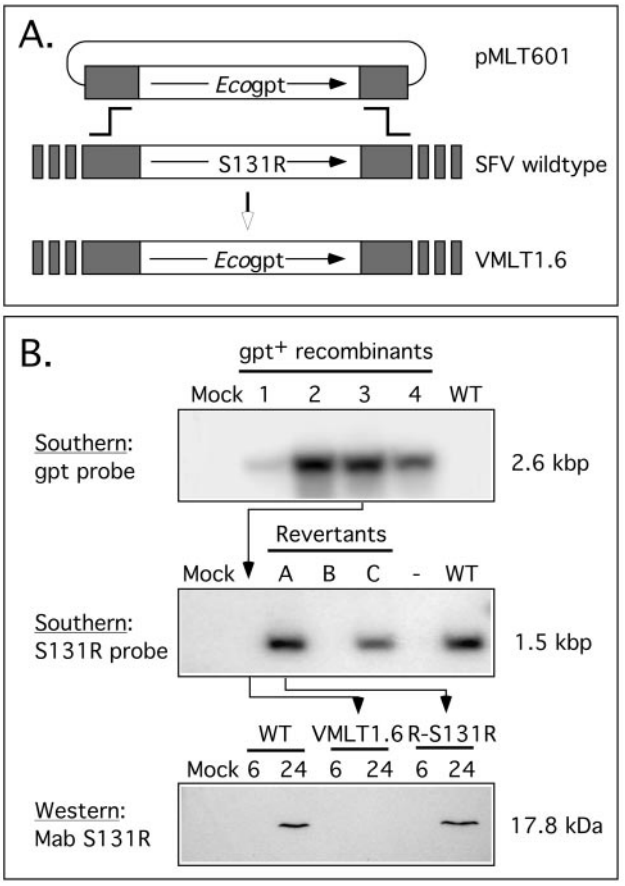

FIG. 1. Construction and characterization of recombinant SFV strains. Plasmid pMLT601 was transfected into wild-type SFV-infected SIRC cells by the calcium phosphate method, and mycophenolic acid-resistant recombinants were isolated as outlined in Materials and Methods. This replaced the S131R gene and its promoter with an *E. coli gpt* cassette. (A) Digestion of these virus DNAs with XbaI followed by Southern blotting detected a 2.6-kb fragment in several independently isolated clones, which hybridized with an *E. coli gpt* probe (B, top). Virus isolate 3 was designated VMLT1.6 and retained for use as an S131R-deficient virus. The S131R gene was restored to VMLT1.6 by using a second round of transfection and recombination using wild-type SFV DNA encoding the S131R gene and flanking sequence homology. Digestion of these revertant viruses with XbaI followed by Southern blotting with an S131R gene probe detected a 1.5-kb fragment diagnostic of wild-type S131R gene structure (B, middle). Virus isolate A was designated R-S131R. A Western blot assay showed that this revertant virus expressed normal levels of S131R gene product with normal (late) expression kinetics; however, no S131R protein was detected in cells infected with the VMLT1.6 virus (B, bottom).

MATERIALS AND METHODS

Cells and viruses. Rabbit corneal fibroblast cells (SIRC cells) and monkey cells (BGMK cells) were grown in Dulbecco's modified Eagle's medium supplemented with 10% fetal bovine serum as previously described (31). SFV strain Kasza and MYX strain Lausanne were originally obtained from the American Type Culture Collection. The construction of a MYX virus lacking the M131R gene (MYX M131RΔ) was described previously (9); it encodes an *Escherichia coli gpt* cassette replacing the M131R gene. Viruses were purified by sucrose density gradient ultracentrifugation and diluted in phosphate-buffered saline (PBS), and titers were determined on SIRC cells before use in animals. Human T-cell lymphoma Jurkat cells were obtained from M. Barry (University of Alberta) and grown in RPMI 1640 medium supplemented with 10% fetal bovine serum (53).

Construction of recombinant viruses. An SFV strain lacking S131R was constructed as outlined in Fig. 1. Plasmid pMLT601 comprises 515 bp of SFV DNA located upstream and 455 bp located downstream of the S131R gene. These flanking sequences were prepared using PCR and the primers S131R-LFF plus S131R-LFR2, S131R-RFF2, and S131R-RFR (Table 1). A tripartite recombinational cloning reaction was then used to join the two flanking fragments to NotI-digested pBluescript KS(+) DNA, directed by sequences homologous to the vector and common to the PCR fragments (Table 1) as described elsewhere (56). The resulting plasmid (pMLT601) was then digested with PacI, dephosphorylated, and ligated to an *E. coli gpt* gene regulated by a vaccinia virus P7.5 promoter (5). This plasmid was transfected into SIRC cells infected with wild-type SFV, and the VMLT1.6 virus was isolated by three rounds of passage in the presence of 25 μg/ml mycophenolic acid followed by three rounds of plaque purification without the selection.

An S131R$^+$ revertant virus was prepared by returning S131R gene sequences to VMLT1.6. Primers S131R-LFF and S131R-RFR (Table 1) and PCR were used to amplify a 1.5-kb DNA fragment encoding the S131R gene and flanking sequences, and the DNA was cloned into pBluescript KS(+) as described above. The resulting plasmid (pMLT701) was then transfected into VMLT1.6-infected cells, progeny virus was harvested 5 days later, and these viruses were plated without mycophenolic acid selection on SIRC cells under an agar overlay. About 100 of these plaque-purified virus isolates were then screened for sensitivity to mycophenolic acid. The drug-sensitive virus that was isolated using this method was then plaque purified two more times and designated R-S131R.

MYX virus encoding M131R linked to the enhanced green fluorescent protein (EGFP) were prepared using a combination of PCR and PCR fusion methods to assemble a gene targeting cassette and homologous recombination to generate the virus. Briefly, primers C/N1F plus C1R and primers C2F and C5R were used to prepare PCR fragments encoding a portion of M130R plus M131R (using a cloned MYX DNA template) and EGFP (using a pEGFP-C3 template [BD/Clontech]), respectively. These were then linked into a single DNA fragment using a PCR fusion reaction and primers C/N1F and C5R. Similarly, primers C4F plus C4R and C6F plus C/N3R were used to prepare PCR fragments encoding

TABLE 1. Sequences of the oligonucleotides used in this study

Designation	Sequence (5′ to 3′)[a]
S131R-LFF	ACTAGTTCTAGAGCGGCCATTACGTACCCTCTAGAACCCATAGG
S131R-LFR2	CGAAGAACGTTAATTAAAGTACGCTACATTATAGATAACTAAACGATAAATAAGCG
S131R-RFF2	TAGCGTACTTTAATTAACGTTCTTCGGGAGTTGCTTAAATAATTTTGCTAAAATATATAAG
S131R-RFR	AGCTCACCGCGGTGGCGGCCCTACTCTACTGTTGCTTTGTCGTT
C/N1F	ACTAGTTCTAGAGCGGCCGGATCCTGCGTATATTATACACGGCC
C1R	TCCTCGCCCTTGCTCACCATGGCGCCAGCAACTCCTATAATCCCCCAG
C2F	CTGGGGGATTATAGGAGTTGCTGGCGCCATGGTGAGCAAGGGCGAGGA
C4F	GCATGGACGAGCTGTACAAGTAACTAAACGGGTCTTGAGGGGT
C5R	ACCCCTCAAGACCCGTTTAGTTACTTGTACAGCTCGTCCATGC
C4R	ATACATTTTAGCGAGGTTATGATGGCATTTCTTCTGAGCA
C6F	TGCTCAGAAGAAATGCCATCATAACCTCGCTAAAATCTAT
C/N3R	GCTCCACCGCGGTGGCGGCCTCTAGAGGGGGAATCTACTCTACTGTT

[a] Underlined portions are sequences homologous to the vector and common to the PCR fragments.

the *E. coli gpt* gene (using pTM3 template [5]) and M132L (using a MYX DNA template), respectively. These were linked into a single DNA fragment using a PCR fusion reaction and primers C4F and C/N3R. These two fragments were then joined using another fusion reaction and primers C/N1F and C/N3R. This 3.9-kbp DNA was transfected into MYX-infected cells, and virus resistant to mycophenolic acid was isolated and plaque purified. The structure of the resulting virus is illustrated below in Fig. 9.

Growth curve analysis. Confluent monolayers of SIRC cells were infected with each virus at a multiplicity of infection of 0.1. After 1 h at 37°C, the cells were washed and overlaid with fresh medium. Virus was harvested over the next 2 days (see Fig. 2, below) and stored frozen at −80°C. The viruses were released by three rounds of freeze-thaw, clarified by centrifugation at 1,500 × *g* for 5 min, and plated on SIRC cells. The cells were cultured for 5 days at 37°C, and plaques were visualized using a 15-min incubation with crystal violet stain (2% formaldehyde, 2% acetic acid, 20% ethanol, and 0.5% crystal violet in PBS) followed by a rinse with PBS.

Southern and Western blot analyses. DNA was extracted from virus-infected cells, cleaved with XbaI, fractionated using a 0.8% agarose gel, and transferred to a nylon membrane (Bio-Rad). PCR-amplified DNAs, [α-^{32}P]dCTP, and a random-prime labeling kit were used to prepare radioactive probes as directed by the kit supplier (Boehringer Mannheim). For Western blot analysis, cells were infected with virus at a multiplicity of infection of 10 and cell extracts were prepared 24 h postinfection as described previously (9). Proteins were fractionated by sodium dodecyl sulfate-polyacrylamide gel electrophoresis (SDS-PAGE) and transferred electrophoretically to a polyvinylidene difluoride membrane as recommended by the manufacturer (Millipore). Western blotting was performed as described previously (9) using a 1:2,000 dilution of a monoclonal antibody that reacts with both the MYX and SFV M/S131R gene products. The primary antibody was detected using a 1:20,000-diluted goat anti-mouse horseradish peroxidase conjugate and a chemiluminescence detection kit (Pierce).

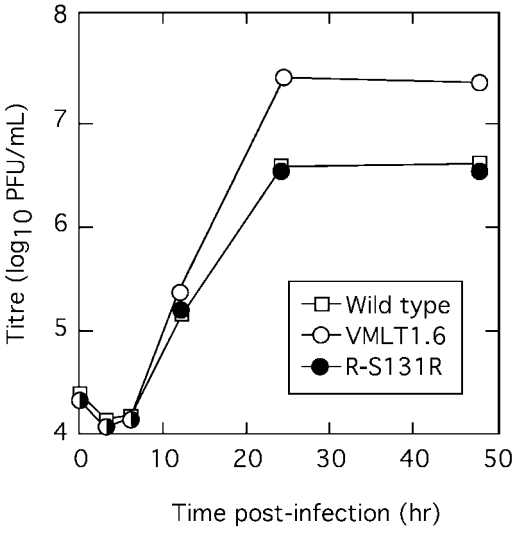

FIG. 2. Single-step growth properties of an S131R-deficient SFV strain. SIRC cells were infected with the indicated virus isolates at a multiplicity of infection of 0.1. Viruses were harvested at the indicated times, titers were determined on SIRC cells, and plaques were detected with a crystal violet stain. Although each virus sample titer was determined in triplicate, the calculated standard error bars were about the size of the data points and have thus not been plotted. All three viruses exhibited similar growth kinetics but, like M131R-deficient MYX strains (9), the S131R mutant viruses grew significantly better in culture.

Confocal microscopy. SIRC cells were cultured on glass coverslips and infected with virus at a multiplicity of infection of 20. The next day (24 h postinfection) the cells were washed with PBS and incubated in fresh medium containing 5 μM hydroethidine (HE; Molecular Probes) at 37°C for 20 min. The cells were washed with PBS and then further stained with 1 μg/ml 4′,6′-diamidino-2-phenylindole (DAPI; Molecular Probes) for 5 min at room temperature and washed again, and the coverslips were mounted in PBS containing 75% (vol/vol) glycerol. To stain cells for SFV antigens, we used the method described in reference 9. A duplicate set of virus-infected cells was fixed and incubated with a primary antibody (1:50-diluted anti-SFV antiserum) followed by a secondary reagent consisting of a 1:400-diluted goat anti-rabbit antibody conjugated with Alexa Fluor 488 (Molecular Probes). These cells were subsequently also stained with DAPI as described above.

Viral pathogenesis. Young adult female New Zealand White rabbits (three virus-infected groups, with six animals per group) were injected intradermally with 50 μl of PBS containing 10^5 PFU of sterile virus in the shaved skin of the back. The rabbits were observed daily for any symptoms of stress, temperature changes, and tumor size. Tumor appearance was documented by digital photography. Tumor volumes were subsequently calculated using the formula $V = [(\pi/24) \times \text{length} \times (\text{width} + \text{height})^2]$. On days 7, 10, and 13, one rabbit from each treatment group was sedated with acepromazine (0.2 mg/kg of body weight) and butorphanol (0.2 mg/kg) intramuscularly, and tumors were biopsied using a 6-mm punch. The tissues were fixed, sectioned, and stained with hematoxylin and eosin for light microscopy. A pathologist blinded as to treatment groups scored the histological appearance on a scale of 0 to 3 (maximum total score = 12) for each of the following changes: edema (abnormal fluid accumulation), inflammation (influx of inflammatory cells), necrosis (destruction of normal tissue components and architecture), and fibromatous cell proliferation (proliferative changes characteristic of SFV infection). All procedures were reviewed, approved, and supervised by the University of Guelph Animal Care Committee operating under the mandate of the Canadian Council for Animal Care.

Aconitase assays. BGMK or SIRC cells were infected with the indicated viruses at a multiplicity of infection of 20. The next day (24 h postinfection) the cells were washed with PBS and harvested by centrifugation at 16,000 × *g* for 5 min at 4°C. The method of Gardner and Fridovich was used to measure aconitase activity (19). Briefly, each cell pellet was resuspended in ice-cold lysis buffer containing 50 mM Tris · HCl (pH 7.4), 0.6 mM $MnCl_2$, and 20 μM fluorocitrate. The cells were broken by sonication on ice (three times for 1 min each) and clarified by centrifugation at 16,000 × *g* for 5 min at 4°C. Aliquots of this supernatant were immediately assayed for aconitase activity by following the ΔA_{340} in a 500-μl reaction mixture containing 50 mM Tris · HCl (pH 7.4), 30 mM sodium citrate, 0.6 mM $MnCl_2$, 0.2 mM $NADP^+$, and 1 U/ml of isocitrate dehydrogenase (Sigma-Aldrich). Reaction mixtures were incubated for 1 h at

20°C with automated absorbance measurements at 5-min intervals. Relative changes in [$O_2\cdot^-$] were calculated from equation 3 in reference 20 and assumed that, in cells infected with M/S131R-deficient viruses, background levels of superoxide reversibly inactivated 14% of the aconitase.

Apoptosis. Jurkat cells were infected, or mock infected, with virus for 24 h at a multiplicity of infection of 10. Apoptosis was induced by adding either 2 μM staurosporine (Sigma-Aldrich) or 250 ng/ml anti-Fas antibody (Upstate Biotechnology) to the culture medium. As a negative control, we added 20 μM of the caspase inhibitor zVAD.fmk (Promega) to the medium prior to inducing apoptosis. The cells were harvested 3 and 10 h posttreatment with staurosporine and anti-Fas antibody, respectively, and assayed for apoptotic induction as follows.

DNA laddering patterns were evaluated by agarose gel electrophoresis (23). Briefly, 10^6 cells from each sample were harvested by centrifugation and the cell pellets were incubated for 1 minute in 0.1 ml of ice-cold lysis buffer (50 mM Tris · HCl [pH 7.5], 1% NP-40, 20 mM EDTA). Each sample was centrifuged for 1,600 × *g* for 5 min, the supernatant was recovered, and SDS and RNase A were added to final concentrations of 1% and 10 mg/ml, respectively. The samples were incubated for 1 h at 50°C, proteinase K was added to a final concentration of 2 mg/ml, and samples were further incubated at 37°C overnight. The DNA was ethanol precipitated and fractionated by electrophoresis using a 1.5% agarose gel. Alternatively, we used a Roche Diagnostics TUNEL (terminal transferase-mediated dUTP-fluorescein nick end labeling) assay kit to detect apoptotic DNA cleavage. Again, 10^6 cells were collected by centrifugation and the cell pellets were washed with PBSF (PBS containing 1% fetal calf serum). The cells were fixed with 2% paraformaldehyde in PBS for 30 min at room temperature, washed with PBSF, and then permeabilized with 0.1% sodium citrate containing 0.1% Triton X-100 on ice for 2 min. The cells were again washed twice with PBSF, resuspended in 50 μl of a solution containing 45 μl of TUNEL label and 5 μl of TUNEL enzyme, and incubated at 37°C for 1 h. The unincorporated label was removed by washing with PBSF, and the cell pellets were finally resuspended in 0.4 ml of PBSF. A Becton Dickinson FACScan was used to determine the distribution of the TUNEL label using at least 10,000 cells per sample.

To detect caspase 3 activation, whole-cell lysates were prepared by boiling 10^3 infected cells in 50 μl of SDS-PAGE loading buffer (containing 2% mercaptoethanol) for 5 minutes. Ten microliters of each extract was then subjected to Western blot analysis, as described above, using a 12% SDS-PAGE gel and a 1:5,000 diluted polyclonal rabbit anti-caspase 3 antibody with chemiluminescence detection.

RESULTS

Construction and characterization of S131R-deficient SFV. Homologous recombination was used as outlined in Materials and Methods to replace the entire S131R open reading frame with sequences encoding an *E. coli gpt* gene as a positive selection marker (Fig. 1A). After plaque purification, the PCR was used to identify potential recombinants, and then Southern blot assays were used to confirm the expected presence of a ~2.6-kbp XbaI recombinant fragment in all of the mycophenolic acid-resistant virus genomes (Fig. 1B). The resulting virus with S131R deleted was designated VMLT1.6. A second round of recombination was then used to restore the S131R gene to VMLT1.6. This produce a wild-type revertant virus, designated R-S131R, which was used as a control to ensure that only the S131R gene was disrupted during construction of VMLT1.6. R-S131R genomic DNA was digested with XbaI, and Southern blot assays were used to detect the presence of a ~1.5-kbp restriction fragment, which is diagnostic of the restoration of the S131R gene (Fig. 1B, middle). Western blot assays were subsequently used to monitor expression of the S131R protein. The 17.8-kDa S131R protein was detected in SIRC cells infected by wild-type SFV and R-S131R virus, using a monoclonal antibody, but absent in extracts prepared from cells infected with S131R-deficient virus (Fig. 1B, bottom). Collectively, these data showed that the recombinant viruses have the predicted genome structure and gene expression patterns.

Growth properties of S131R-deficient viruses. The phenotypic properties of S131R-deficient SFV strains closely resembled the properties of MYX strains with M131R deleted (9). The gene is clearly dispensable for virus replication in tissue culture and, like M131R-deficient MYX strains, the size and morphology of the foci formed by VMLT1.6 virus on SIRC cells were indistinguishable from those of the SFV-WT and R-S131R strains (data not shown). The S131R-deficient SFV virions also shared with mutant MYX strains some thermolability at elevated (55°C) temperatures (57). Perhaps the most interesting property of these viruses, and one that again characterizes M131RΔ MYX virus (9), is that deleting the S131R gene enhances the yield of SFV. This is illustrated by the single-step growth curve shown in Fig. 2. Starting with a low multiplicity of infection (0.1), all three viruses exhibited the same growth characteristics during the first 12 h postinfection. However, the VMLT1.6 infection ultimately produced about 10-fold more infectious particles than either the wild-type or R-131R strains. Even though SFV and MYX appear to be evolutionarily distinct viruses (8, 55), these results illustrate the apparent biological equivalence of the two orthologous genes.

The S131R gene product perturbs steady-state intracellular superoxide concentrations. To test whether the S131R protein plays any role in regulating intracellular superoxide concentrations, we examined the effect of virus infection on the fluorescent properties of HE dye. HE reacts with superoxide to produce a compound resembling ethidium bromide, which then forms a red fluorescent product (59). This product can be detected by confocal fluorescent microscopy using cells infected with different SFV strains and stained with HE dye (Fig. 3). Our analysis showed that cells infected with wild-type SFV contained higher amounts of intracellular superoxide, relative to mock-infected cells, as judged by the stronger staining in SFV-infected cells. Mock-infected cells showed only a low level of HE staining, indicating a low basal level of production of $O_2\cdot^-$ by cellular metabolism. This phenotype was clearly dependent upon S131R gene function, since deleting S131R produced only a background level of HE staining in VMLT1.6-infected cells while cells infected with R-S131R revertant virus exhibited wild-type levels of superoxide-dependent HE fluorescence.

A high multiplicity of infection was used in these experiments to ensure that all cells were infected with SFV (20 PFU per cell); however, these studies could have been confounded by the failure of VMLT1.6 virus to infect the majority of cells being imaged. To show that these cells were all more or less equally infected with virus, we also stained the cells with convalescent antibodies recovered from rabbits that had been experimentally infected with wild-type SFV (see below). This immunolabeling of SFV antigens was done in parallel with HE staining, because HE staining must be conducted in live cells while immunolabeling requires a fixation step. The convalescent-phase serum contained a high level of anti-SFV immunoglobulin G antibodies and detected the presence of cytoplasmic SFV antigens in essentially all of the cells in these infected monolayers (Fig. 3, bottom panel). No cross-reactive antigens were detected in mock-infected cells. This result showed that variations in infection efficiency do not explain the effects different viruses have on cellular superoxide levels.

Although HE is recognized as one of the better reagents

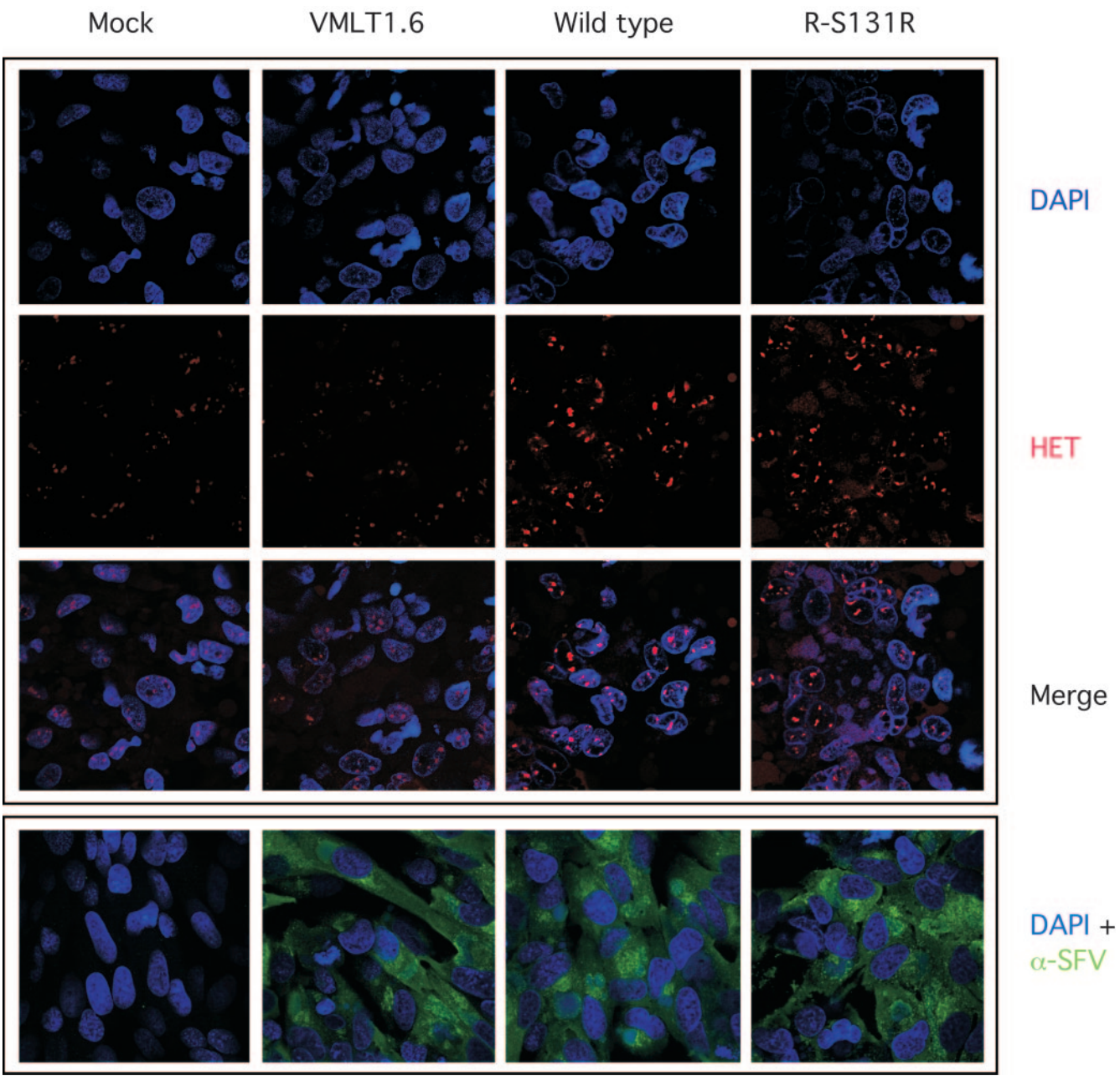

FIG. 3. The S131R gene promotes an increase in the amount of intracellular superoxide radical in SFV-infected cells. SIRC cells were infected, or mock infected, with the indicated virus and then stained with HE and DAPI to detect superoxide and DNA, respectively. A background level of superoxide was detected in mock-infected cells, which did not appear to be altered by infection with the VMLT16.6 virus (columns 1 and 2). Elevated levels of superoxide were detected in cells infected with wild-type and R-S131R revertant virus-infected cells, as judged by an increase in the amount of HE fluorescence (columns 3 and 4). As an infection control, a parallel set of infected, or mock-infected, cells were labeled with a polyclonal antiserum obtained from an SFV-infected rabbit, followed by detection with a secondary antibody conjugated with Alexa Fluor 480. SFV antigens were detected in all of the infected specimens. Note that superoxide converts HE into a fluorescent intercalating dye of imperfectly understood structure and that this is detected by the subsequent staining of nucleic acids (59). The distribution of HE stain thus does not reflect the original cellular distribution of superoxide.

available for detecting superoxide, the method can underestimate the rate of $O_2\cdot^-$ production due to HE-catalyzed superoxide dismutation (48). Another well-validated method is based upon the observation that superoxide can reversibly strip the metal from [4Fe-4S] clusters and thus inhibit iron-sulfur enzymes like aconitase. We used a photometric method (19) to assay aconitase activity in extracts prepared from SFV-infected cells, and the data obtained using this method were in full agreement with results obtained using HE. These results are presented in Fig. 4. Infection caused a general reduction in aconitase levels, relative to mock-infected cells, but superimposed upon this cytopathic effect was the observation that

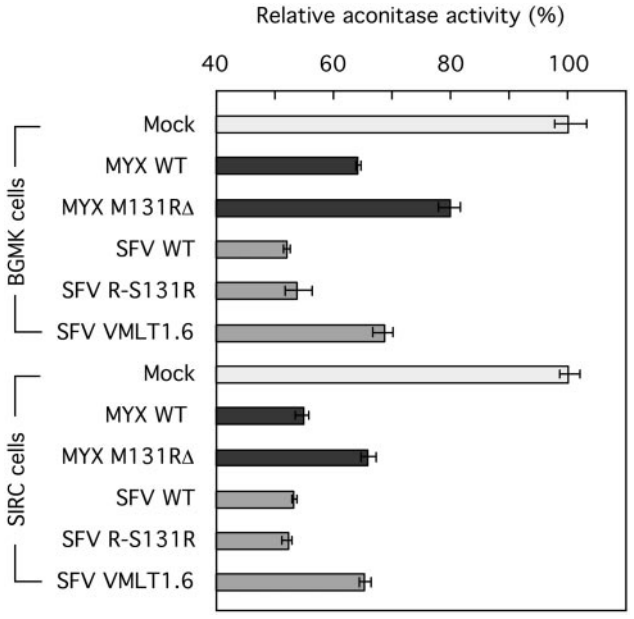

FIG. 4. Detection of intracellular superoxide using an aconitase inhibition assay. A spectrophotometric method was used to measure the activity of the superoxide-sensitive enzyme aconitase in extracts prepared from virus-infected cells. Infection caused a nonspecific reduction in cytosolic aconitase activity relative to the activity detected in mock-infected BGMK and SIRC cells. In addition to this effect, any virus encoding M131R or S131R caused an additional 12 to 15% reduction in aconitase activity relative to that in cells infected with mutant viruses lacking these genes.

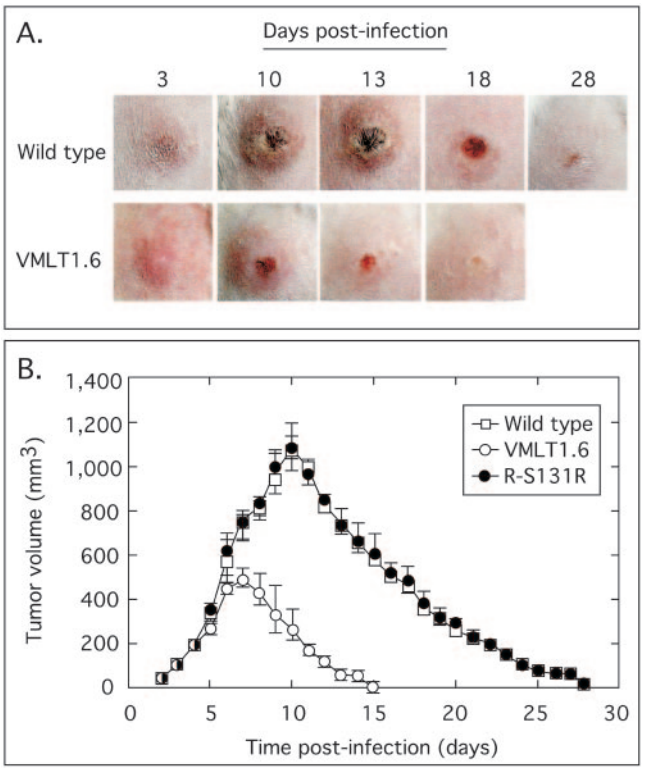

FIG. 5. Deleting the S131R gene attenuates SFV-induced disease in rabbits. New Zealand White rabbits were inoculated intradermally with 10^5 PFU of wild-type, VMLT1.6, or R-S131R revertant virus on a shaved area at the back of each animal. The resulting tumors were monitored daily and recorded with a digital camera (A), and the tumor volume was determined with a digital calliper (B). Virus lacking the SFV S131R gene produced smaller tumors, which regressed much faster than those produced by wild-type and revertant viruses (B). There was also less inflammation, hemorrhaging, and necrosis accompanying the resolution of infections caused by mutant virus relative to wild-type infections (A). Note that a total of six animals were used in each group, but as one animal from each group was biopsied on days 7, 10, and 13 the animal was excluded from further measurements of tumor progression. R-S131R virus produced tumor-like growths identical to wild-type SFV, and these images have therefore been omitted from panel A.

extracts from cells infected with SFV wild-type and R-S131R viruses contained 12 to 15% less aconitase than did extracts prepared from cells infected with the VMLT1.6 S131RΔ virus. These differences were seen in both rabbit and monkey cells and were clearly statistically significant ($P \leq 0.005$ for SFV wild-type versus VMLT1.6 viruses [Student's two-tail t test, $n = 3$]). The same effects were also seen using cells infected with mutant and wild-type MYX viruses (Fig. 4). Based upon these two independent approaches for detecting intracellular superoxide, we concluded that the M/S131R genes serve a role in up-regulating superoxide levels in virus-infected cells.

S131R is a virulence factor that promotes tumorigenesis in rabbits. To examine whether the S131R gene serves any role in modulating SFV pathogenicity, we inoculated young adult female New Zealand White rabbits with VMLT1.6 virus and compared the clinical manifestations of the disease with those induced by wild-type and R-S131R revertant virus. Before initiating these experiments, the wild-type virus was used in a small pilot experiment to determine the infectious properties of our SFV laboratory stock (strain Kasza) and to identify an appropriate infectious dose. Three different doses of virus were injected intradermally into nine New Zealand White rabbits (10^4, 10^5, and 10^6 PFU per animal, in triplicate), and the kinetics of tumor induction was then followed over 3 weeks. We identified 10^5 PFU as an appropriate inoculum, since a 10-fold higher dose produced no further effects on the disease progression while 10^4 PFU per rabbit caused smaller growths and a less synchronized rate of tumor induction (data not shown).

Our wild-type SFV produced the classical fibroxanthosarcomatous tumors in rabbits that have been described in the literature (32, 41). These tumors were limited to the site of inoculation (the rear flank) with no evidence of systemic spread to other sites in these animals. Photographs were taken daily to monitor the course of the infection, and Fig. 5A (top) shows the pattern of tumor growth and recession following the inoculation of one representative rabbit with wild-type virus. Lesions began to appear on day 3 postinfection, and the tumor-like growths reached a maximum size by about day 10. The lesion became hemorrhagic and then necrotic by day 13, at which point tumor regression also began to be noted. The tumors continued shrinking, and the thick scalp caused by the necrosis eventually sloughed off, leaving a small residual scar. The infection was completely resolved by day 28 postinfection. Wild-type and R-S131R virus produced indistinguishable disease progressions. In contrast, although VMLT1.6 virus still established an infection, the size of the tumor formed by this

virus was greatly reduced by deleting the S131R gene (Fig. 5A, bottom). These tumor-like growths appeared with about the same kinetics as in wild-type infections, but the tumors were much smaller and reached a maximum size at an earlier time point (day 7 instead of day 10). It is also noteworthy that the hemorrhagic and necrotic phases were less extensive in VMLT1.6-infected animals, with virtually no dark necrotic scars. Tumor regression was rapid, and these animals completely resolved the infection by day 18 postinoculation.

Tumor size measurements were also determined in parallel with these visual studies and are presented in Fig. 5B. A total of six animals per group were followed, although as a biopsy was taken at different time points from each of three animals in each group (see below), the animal was removed from further calculations of tumor volume. Tumors from all three groups grew at a similar rate during the first 5 days after inoculation, and those produced by wild-type and R-S131R virus continued to grow rapidly until they reached essentially identical maximum sizes of 1,070 ± 80 mm^3 and 1,080 ± 60 mm^3 (means ± standard errors) for wild-type and R-131R viruses, respectively, by day 10 postinfection. In contrast, the growth rate of tumors produced by S131R-deficient virus started to slow by day 5 postinfection and reached a maximum size that was only half that of the wild-type virus (500 ± 40 mm^3) by day 7 postinfection. These smaller tumors also cleared in half the time compared with those seen in wild-type and R-131R infections. Thus, S131R-deficient virus produces significantly smaller tumors than do wild-type or R-S131R virus ($P = 3 \times 10^{-4}$ and 4×10^{-3}, respectively, at day 7 versus day 10 [Student's two-tail t test, $n = 4$]).

Histologic studies on tumor biopsies. To observe the cellular response to virus infection, tumor biopsies were performed at different time points and subjected to microscopic evaluation. A lesion scoring system was established (see Materials and Methods) that provided a semiquantitative measure of the extent of pathology at time points permitted by our animal utilization protocol. By day 7 postinfection, all three treatment groups exhibited identical lesion scores (score = 6) consistent with there being no obvious microscopic differences in the appearance of the tumors (Fig. 6A, B, and C). We saw ulcerated skin masses overlying the injection sites, and this correlated histologically with a locally extensive full-thickness epithelial necrosis. All three specimens had an overlying crust consisting of necrotic cell debris mixed within a proteinaceous exudate. The subcutis subtending this area was edematous with marked perivascular and periadnexal mixed leukocytic infiltrates (Fig. 6J). These infiltrates comprised a mixture of heterophils, macrophages, and lesser numbers of lymphocytes and plasma cells. Rare intranuclear inclusion bodies were seen in perifollicular cells of animals treated with wild-type virus (Fig. 6H).

By day 10 postinfection, we started to see obvious histologic differences between the specimen obtained from a VMLT1.6-infected animal (lesion score = 6) and those obtained from the other two control animals (lesion scores = 8) (Fig. 6D, E, and F). Little change was seen in the necrotic epithelial lesion produced by the VMLT1.6 virus, beyond a mild increase in dermal necrosis and a decrease in perivascular edema. There was no evidence of fibromatous cell proliferation. In the other two groups the lesions had continued to progress. In addition to a superficial epithelial necrosis, extensive areas of superficial and deep dermal inflammation with dense mononuclear cell infiltrates were observed. These were associated with the disruption and loss of hair follicles and adnexal structures and dermal necrosis admixed with hemorrhage and edema. Additionally, there were scattered areas of deep dermal fibromatous cell proliferation (Fig. 6L) and mesenchymal cell disorganization within a classical myxoid tumor stroma.

By day 13, the tumors from animals in the VMLT1.6 group were resolving and regressing histologically (lesion score = 4) with abnormalities limited to residual mononuclear leukocytic infiltrates in superficial areas of the biopsied section (Fig. 6G). In contrast specimens obtained from the wild-type and R-S131R groups showed evidence of continued disease progression with pending tissue rejection and subsequent sloughing (lesions scores = 9 and 10 for R-S131R and wild-type infections, respectively) (Fig. 6H and I). We also noted extensive and well-demarcated areas of superficial and deep dermal necrosis with marked mononuclear cell infiltrates, dermal fibrosis and scarring, occasional vascular thromboses, and marked fibromatous proliferation in these sections. Collectively, these observations show that infections initiated by S131R-deficient virus are more rapidly cleared by a cell-mediated immune response and this occurs before the appearance of myxoid stroma and the fibromatous cell proliferation that characterizes wild-type SFV infections.

M131R inhibits both mitochondria-mediated and anti-Fas-induced apoptosis in virus-infected cells. The results outlined above could be explained by the hypothesis that cells infected with S131R-deficient viruses cannot mount an effective defense against a cell-mediated immune response. This response often targets virus-infected cells for killing by apoptotic processes, and the superoxide anion that is up-regulated during virus infection (Fig. 3) is known to suppress apoptosis triggered through the Fas receptor pathway (10, 11). Therefore, we decided to test whether leporipoxvirus SOD1 homologs might serve an antiapoptotic function in virus-infected cells. These experiments were performed using human T-lymphocyte Jurkat cells and MYX instead of SFV. Jurkat cells provide a well-characterized model for studying apoptotic processes, and suitable reagents are widely available for use with human cells. MYX virus was used because Jurkat cells can support MYX growth, but not that of SFV. As noted above, the genetic and biochemical properties of the MYX and SFV M/S131R homologs seem to be identical, and we also confirmed that MYX infection of Jurkat cells up-regulates the steady-state superoxide concentration in an M131R-dependent manner (see Fig. 9).

Jurkat cells were treated with either staurosporine or anti-Fas antibodies to induce either the mitochondrial- or death receptor-mediated pathways of apoptosis, respectively. Both treatments efficiently induced apoptosis as illustrated by the fragmentation of chromosomal DNA into nucleosome-sized fragments and the subsequent detection of this apoptotic ladder by agarose gel electrophoresis (Fig. 7A). In contrast, when cells were infected with wild-type MYX for 24 h prior to the induction of apoptosis, no DNA fragmentation was observed following either treatment. Most importantly, this effect seemed to be dependent upon M131R function, since deleting the gene permitted near-normal levels of staurosporine-in-

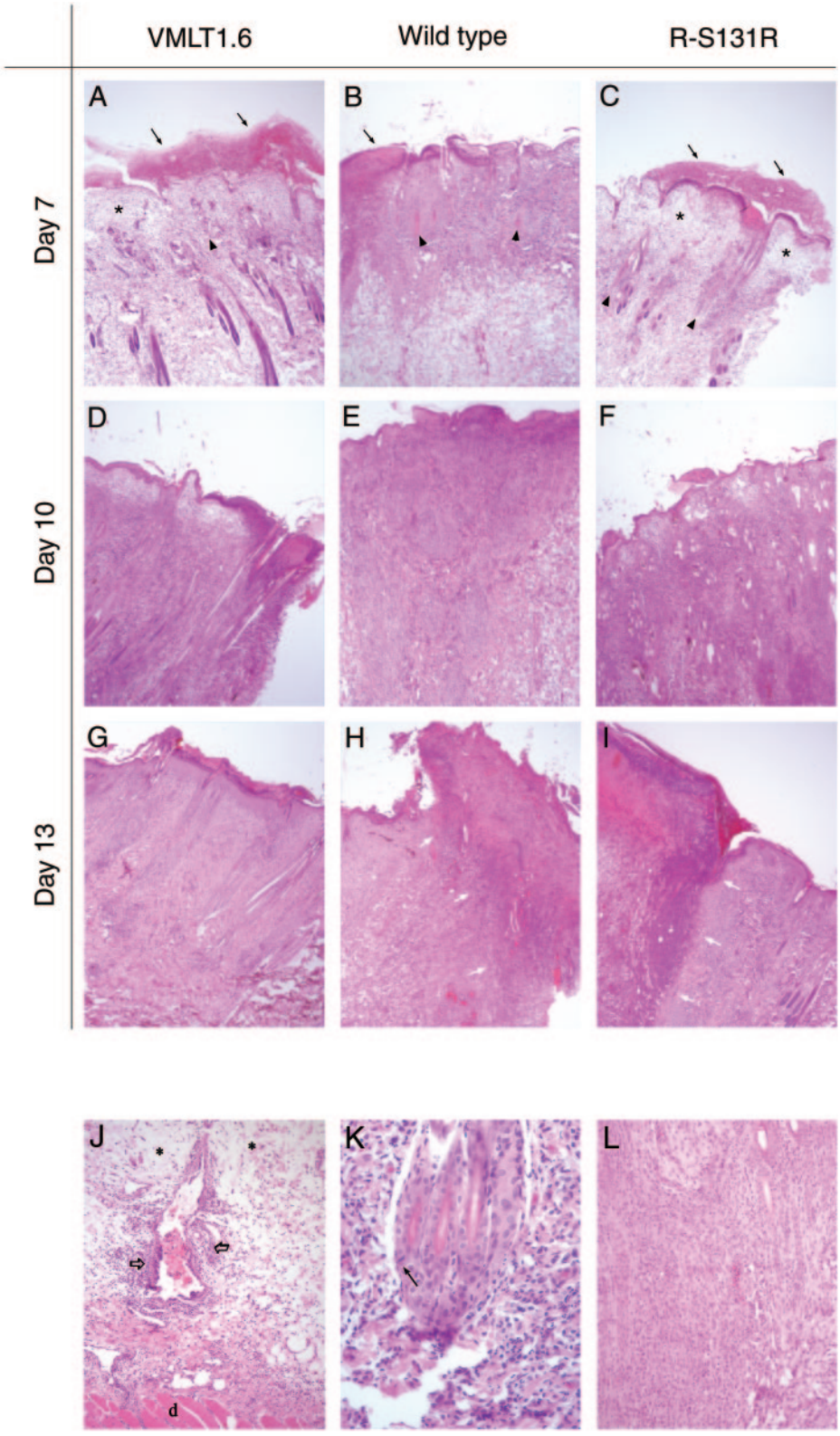

FIG. 6. Histologic analysis of tumors induced by wild-type, VMLT1.6, and R-S131R viruses. Tumors were biopsied on the days indicated and stained with hematoxylin and eosin for light microscopy. Specimens have been oriented to place the ulcerated epithelium (thick red crust) on the top (A, B, and C) (arrow) and the deeper dermal layers at the bottom (J) (deep dermis is delineated by "d"). The pale, clear areas throughout the tissue sections represent areas of edema (A, C, and J) (asterisks), while the more basophilic areas (dark purple/blue areas) represent areas of mixed leukocytic infiltration. On day 7 postinfection no differences were noted in tumor appearance between any of the treatment groups. Rare eosinophilic intranuclear inclusion bodies were noted in perifollicular cells of animals infected with wild-type virus (K) (arrow). On day 10, the

duced apoptosis and normal levels of Fas-mediated apoptosis (Fig. 7A). Control experiments showed that neither mutant nor wild-type virus infection could trigger apoptosis in Jurkat cells in the absence of an apoptotic inducer. We also treated these cells with a broad-spectrum caspase inhibitor, zVAD.fmk, and this compound blocked the appearance of an apoptotic DNA ladder in samples treated with the apoptotic stimulants (Fig. 7B).

To investigate more closely the impact of M131R on this process, we examined the fate of caspase 3 by Western blot analysis. Caspase 3 is one of the key downstream effector molecules in the proteolytic cascade. Treating mock-infected Jurkat cells with 2 μM staurosporine or 250 ng/ml of anti-Fas antibody resulted in the cleavage and activation of caspase 3 as revealed by the conversion of the 32-kDa proenzyme into a 19-kDa product (Fig. 7C). Caspase 3 activation was also seen in cells infected with the M131RΔ virus, but it was blocked in cells infected by wild-type MYX. To prove that wild-type viruses were establishing a productive infection, we also performed a Western blot assay, looking for expression of the M131R late gene product. The protein was readily detected but, as expected, only in cells infected with wild-type virus (Fig. 7D). These observations suggest that leporipoxvirus SOD1 homologs interfere with apoptotic signaling events at some point upstream of caspase 3 activation.

To further confirm the antiapoptotic function of M131R as well as gain some more quantitative insights into the effectiveness of this immunomodulatory pathway, we performed TUNEL of virus-infected cells followed by fluorescence-activated cell sorter (FACS) analysis. Control experiments showed that treating mock-infected Jurkat cells with anti-Fas antibody for 3 h resulted in 38% of cells becoming TUNEL positive, whereas a 10-h exposure to staurosporine resulted in 29% TUNEL-positive cells (Fig. 8, top). The effectiveness of antiapoptotic MYX gene products is illustrated by the fact that only background levels of TUNEL-positive cells were detected when these cells were first infected with wild-type virus prior to either treatment (Fig. 8, middle). Interestingly, with this assay it can be seen that deleting the M131R gene rendered virus-infected cells partially and perhaps differentially sensitive to both of these exogenous stimuli (Fig. 8, bottom). In the absence of M131R gene function, mutant MYX virus still appeared able to mount a partial defense against staurosporine-triggered apoptosis (~70% of wild type) and a less-effective response to Fas-triggered apoptosis (~40% of wild type). These observations suggest that leporipoxvirus SOD1 homologs can protect type II Jurkat T cells from both mitochondrial and Fas/FasL-mediated apoptotic pathways. However, M/S131R gene function likely acts in concert with the activity

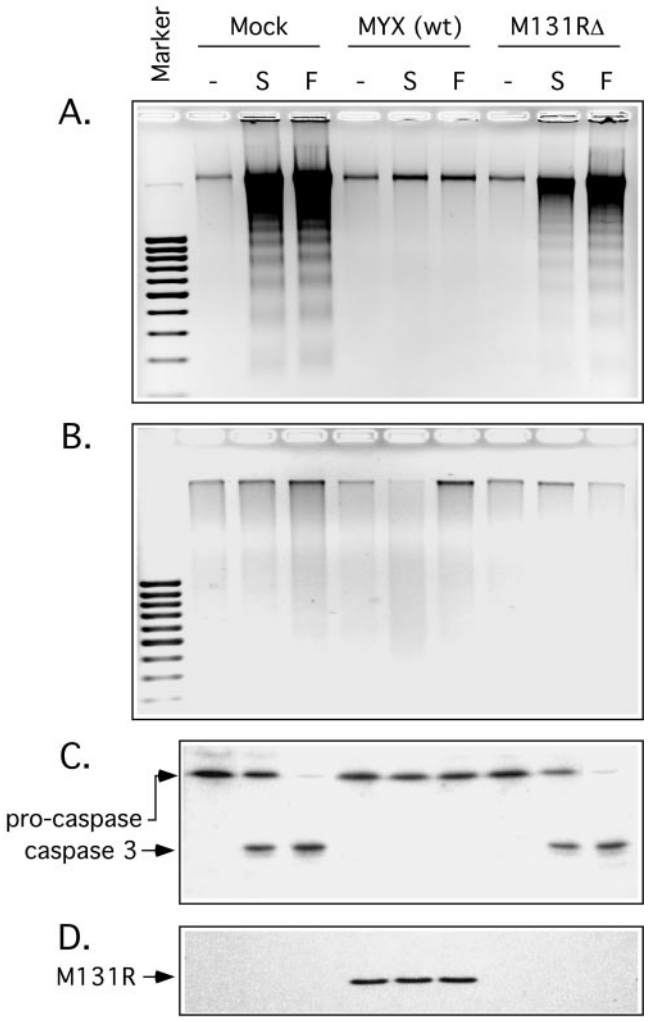

FIG. 7. The MYX M131R gene product protects infected cells from Fas- and staurosporine-induced apoptosis. Jurkat cells were infected for 24 h with wild-type MYX or MYX with M131R deleted and then exposed to staurosporine (S) or anti-Fas antibody (F) for 3 h or 10 h, respectively. Fragmented cellular DNA was extracted, fractionated by agarose gel electrophoresis, and visualized with ethidium bromide. In mock-infected cells, both staurosporine and anti-Fas treatments produced a classical 200-bp nucleosomal ladder indicative of apoptotic induction (a 100-bp size marker is indicated). Wild-type MYX protected Jurkat cells from these effects, but this protection depended upon M131R gene function and was not seen in cells infected with M131RΔ virus (A). As a control we added the caspase inhibitor zVAD.fmk, and this drug completely prevented DNA laddering (B). Western blot analysis showed that DNA laddering correlated with caspase 3 activation and that the virus with M131R deleted could not prevent cleavage of procaspase 3 (C). Another Western blot control showed that the M131R protein was expressed only in cells infected with wild-type MYX virus (D).

necrotic epithelial lesion was relatively unchanged in VMLT1.6-infected animals (D) beyond a mild increase in dermal necrosis and a decrease in perivascular edema. We saw no evidence of fibromatous cell proliferation. In contrast, these lesions had continued to progress in tissues infected with either the wild-type or revertant viruses (E and F, respectively). In addition to superficial epithelial necrosis, extensive areas of superficial and deep dermal inflammation with dense mononuclear cell infiltrates were observed (J) (open arrows denote perivascular infiltrates), with continued disruption and loss of hair follicles and adnexal structures (B and C) (arrowheads mark loss of follicular structures) and dermal necrosis admixed with hemorrhage and edema. By day 13 postinfection, specimens taken from wild-type and revertant virus infections still showed extensive areas of inflammation, necrosis (H and I) (necrotic areas are delineated by white arrows), and proliferation at the site of injection (L), whereas tumors from animals in the VMLT1.6 group were resolving and regressing back to a near-normal state (G).

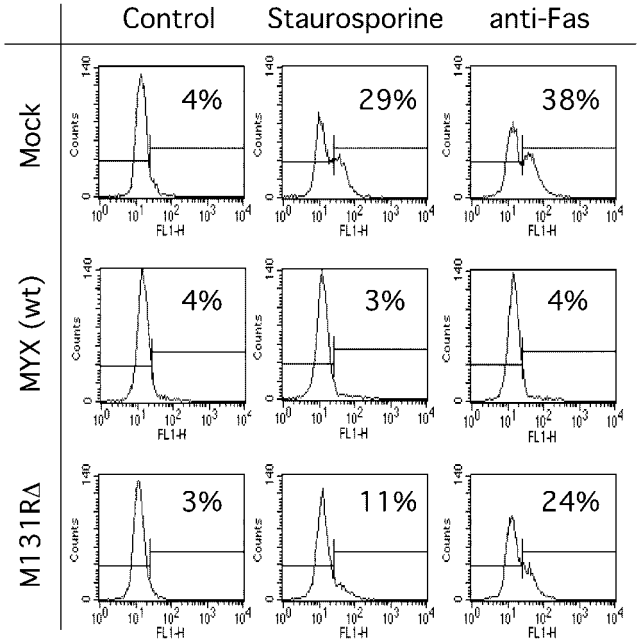

FIG. 8. FACS detection of apoptosis in MYX-infected cells. Jurkat cells were infected, or mock infected, with the indicated viruses and treated with staurosporine or anti-Fas antibodies as described in the legnd for Fig. 7. A TUNEL kit and FACS analysis were then used to identify the percentage of cells undergoing apoptosis. Wild-type MYX infection completely suppressed apoptosis induced by either agent, whereas the deletion of M131R gene function rendered the cells partially susceptible to both stimuli. The M131R gene appeared to play a greater role in protecting cells from anti-Fas treatment, as judged by the relatively greater proportion (24%) of apoptotic cells detected in M131RΔ-infected cells treated with anti-FAS antibody.

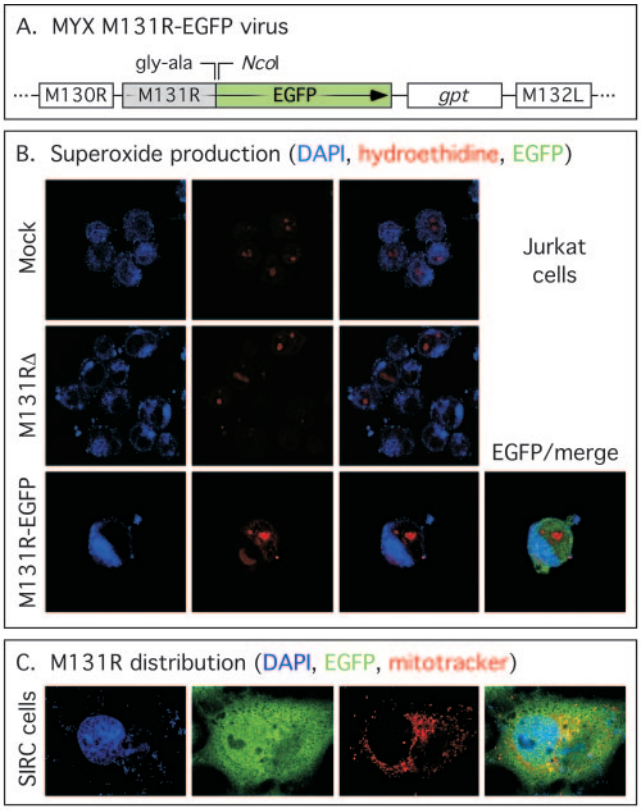

FIG. 9. Distribution of EGFP-tagged M131R protein in virus-infected cells. (A) The MYX M131R-EGFP virus used in these studies. The virus encodes a C-terminal fusion of EGFP to M131R and a *gpt* selectable marker separating the gene encoding the fusion protein from M132L. The M131R-EGFP fusion protein continues to be expressed from the M131R promoter. These MYX viruses were used to infect Jurkat cells at a multiplicity of infection of 10 for 24 h, and then these cells were stained with DAPI or HE to visualize the nucleus and measure the amount of superoxide generated over a 20-min incubation period (B). Note the elevated level of HE dye product seen in cells infected with M131R-EGFP virus. M131R-EGFP fusion protein was also detected in this cell. (C) Comparison of the distribution of M131R-EGFP fusion protein relative to the locations of the nucleus (DAPI) and mitochondria (Mitotracker Red). EGFP-tagged M131R appears to be distributed widely in the cell.

of other previously characterized antiapoptotic gene products, such as M11L (13).

M131R is abundantly expressed and widely distributed throughout infected cells. Finally, in order to gain some insights into where, when, and how M131R might be exerting these antiapoptotic effects, we prepared a recombinant MYX virus encoding EGFP fused to the C terminus of M131R (Fig. 9A). This M131R-EGFP virus was then used to directly monitor the intracellular distribution of M131R without the necessity of fixing and immunostaining the protein, as we had had to do previously (49). The fusion protein was easily detected by Western blot analysis and exhibited a late gene expression pattern identical to that of native M131R protein. The fusion protein also cosedimented with MYX virions though a sucrose density gradient, as does the native protein (data not shown). To test whether the fusion protein was functional, we infected Jurkat cells with the M131R-EGFP virus and stained the cells 24 h postinfection with HE. The dye detected an increase in superoxide abundance in $EGFP^+$ cells relative to the background HE signal detected in mock- and M131RΔ virus-infected cells (Fig. 9B). In these experiments the EGFP signal was also seen distributed throughout the cell cytoplasm, but Jurkat cells are not well suited to localization studies due to their small size.

SIRC cells provided a better model for a distribution analysis. We still could not detect the faint signal that might be expected from delivery of virus-encapsidated M131R-EGFP protein to infected cells, but we could easily detect the late expression of the protein starting 10 to 12 h postinfection. By 24 h postinfection, confocal fluorescence microscopy detected very high levels of a fluorescent protein distributed throughout all parts of the cytosol of infected cells (Fig. 9C). This distribution included the nucleus, a site not well visualized by our previous studies that used fluorescent antibody methods (49). We also compared the distribution of the protein with the distribution of mitochondria. We had previously used immunofluorescence microscopy and cell fractionation methods to examine this question, but we had obtained contradictory data regarding whether cells selectively accumulate M131R within mitochondrial compartments (49). The data presented in Fig. 9C support our earlier biochemical studies in that, although there was some colocalization of a mitochondrial stain and the EGFP-tagged protein, the broad distribution of the fluores-

cence suggested that no one part of the cell is a special target of M131R. SOD1-like leporipoxvirus proteins are produced in abundance during virus infection and seem to act at sites distributed throughout the cell.

DISCUSSION

Poxviruses encode many genes that are not essential for replication in culture but which are important determinants of pathogenicity in vivo (reviewed in reference 38). A characteristic feature of many of these gene products is that they complex with signaling molecules (e.g., cytokines, double-stranded RNAs, or regulatory proteins) and thus interfere directly in the activation of critical antiviral defense pathways. In the present study, we have investigated the biological function of leporipoxvirus SOD1 homologs. We have shown that these genes are not required for virus growth; indeed, M/S131R-deficient viruses actually grow better than does wild-type virus. This cannot be attributed to the presence of the *gpt* marker since, as long as they are not exposed to UV light, MYX viruses encoding the same *gpt* cassette replacing the M127L photolyase gene grow equally well as wild-type MYX (5, 54). We suspect that the phenomenon reflects a role served by the protein in stabilizing the capsid against environmental stressors like desiccation and heat. Such a function is not required under laboratory growth and infection conditions and might conceivably have detrimental effects on virus yields (57). We have also shown that deleting the SFV S131R gene renders SFV less "tumorigenic" in rabbits and that these gene products play a role in suppressing Fas- and staurosporine-triggered apoptosis in cultured cells. Concurrently, we have shown that wild-type MYX and SFV infections normally cause increases in the steady-state intracellular concentration of superoxide anion and that this effect is dependent upon M/S131R gene function. Superoxide anion has been shown to exert both proproliferative and antiapoptotic effects on cells under some circumstances (see below), and our data suggest that tumorigenic poxviruses can gain advantages from these effects by using Cu-Zn SOD1 homologs to indirectly manipulate the concentration of $O_2\cdot^-$ in virus-infected cells.

How $O_2\cdot^-$ affects such diverse phenomena as cell growth, apoptosis, and inflammation is complicated by the "Goldilocks effect" in that either too much or too little superoxide will have deleterious effects on cells and that an optimal growth environment requires a redox state that is "just right." These biphasic effects of redox stress on cellular metabolism, coupled with the genetic diversity of cultured cells, can provide an explanation for the sometimes paradoxical data in the literature (22). It is now generally understood that the activation of cellular receptors by growth factors or cytokines leads to ROS production and that this can trigger a signal transduction cascade in which ROS-sensitive mitogen-activated kinases activate the AP-1 transcription factor via phosphorylation of its c-*jun* and c-*fos* subunits (3, 4, 46). Leporipoxviruses, like most other chordopoxviruses, express functional epidermal growth factor homologs (29, 30). These proteins promote a proliferative response in infected cells and are expected to signal through the ErbB pathway. The proproliferative effects of these viral growth factors would be potentiated by inhibiting cellular SOD1 (and thus stabilizing $O_2\cdot^-$) and account for the reduced fibromatous cell proliferation seen in animals infected with S131R-deficient viruses (Fig. 6). The activity of this gene product would also explain why deleting MYX and malignant rabbit virus growth factor genes doesn't entirely prevent virus-induced tumor formation.

How ROS might regulate apoptosis is less well understood at the molecular level and is further complicated in poxvirus-infected cells, where additional antiapoptotic gene products are also expressed. It is clear that overproduction of superoxide beyond the detoxification capacities of a cell can induce apoptosis or necrosis (7). However, it is unlikely that the increase in $[O_2\cdot^-]$ that is detected using HE staining is very large (Fig. 3), given that infection caused just a 60% drop in the amount of Cu-Zn SOD1 activity (9) and only a modest decrease in the activity of the superoxide-sensitive cellular enzyme aconitase (Fig. 4). The difference in aconitase activity in cells infected with mutant versus wild-type viruses permits the calculation (20) that M/S131R activity changes the steady-state $[O_2\cdot^-]$ only 2.5- or 3.0-fold in SIRC and BGMK cells, respectively, and shows that SFV and MYX infections create only a mildly prooxidative state in virus-infected cells. Under these conditions, there have still been a number of reports showing that superoxide has antiapoptotic effects. For example, treating cells with either paraquat or the SOD1 inhibitor diethyldithiocarbamate caused a two- to threefold increase in intracellular $[O_2\cdot^-]$ that completely suppressed Fas-mediated apoptotic killing of human melanoma cells (11). More recently the ROS produced following exposure to growth factors has also been shown to have antiapoptotic effects in pancreatic cancer cells (50). How this effect is accomplished is still controversial. Vaquero et al. showed that growth factor signaling can activate soluble nonmitochondrial NAD(P)H oxidases to produce superoxide and suggested that this ROS might then activate antiapoptotic genes regulated by NF-κB. NF-κB also activates SOD1 gene expression (33), and so this makes sense from a regulatory perspective. However, this is unlikely to be the whole story, because the AP-1 constituent c-*fos* is an NF-κB-regulated gene (17) and thus the two ROS-sensitive pathways are interlinked at the transcriptional level. SFV and MYX are presumably perturbing this network of exquisitely redox-sensitive systems to their advantage, but our current understanding of these networks suggests that there are many molecular targets.

We also noted that deleting M131R seemed to differentially affect MYX's capacity to suppress both the mitochondrial- and Fas-mediated apoptotic pathways. Wild-type virus inhibited apoptosis in the presence of both agents, but cells infected with M131R-deficient virus retained a greater degree of resistance to apoptosis following staurosporine treatment than was seen following treatment with anti-Fas antibodies. This suggests that M/S131R may serve a relatively more important role in suppressing extrinsic apoptotic signaling. Jurkat cells are type II cells, in which both Fas-mediated and staurosporine-induced apoptosis depend upon the activation of the mitochondrial pathway, and so our data suggest that changes in $[O_2\cdot^-]$ are exerting pleiotropic, but relatively greater, effects on upstream events linking aggregation of the Fas receptor to Bak activation. Caspase 8 activity is ROS sensitive and thus represents at least one possible enzymatic target within this cascade (42). The fact that inactivating M131R does not completely abro-

gate either response is not surprising given that the MYX M11L gene product targets the mitochondrial voltage-gated ion channel and protects virus-infected cells from apoptotic signals mediated by Bak (13, 51). Interestingly, these authors also noted that M11L-deficient virus was still capable of providing significant protection against Fas-mediated apoptosis (13), demonstrating the existence of other MYX-encoded antiapoptotic genes. What this residual defense might be is not explained by the known biological properties of other MYX apoptotic modifiers (M-T2, M-T4, and M-T5) and could be explained by the existence of M131R.

M131R and S131R are not the only known poxvirus gene products that can alter the redox state of infected cells. For example, the molluscum contagiosum MC066L gene encodes a glutathione peroxidase that protects cells expressing the protein from the proapoptotic peroxides generated by UV light (40). Poxviruses also catalyze the oxidation of disulfide bonds in virus proteins by using a network of redox-active proteins (39). Whether other poxvirus SOD1 homologs all serve the same function as M/S131R is doubtful, since the SOD1 homolog encoded by *Amsacta moorei* entomopoxvirus is catalytically active and likely serves an entirely different function in virus-infected insects (2). Many other virus infections have also been reported to disrupt cellular ROS homeostasis, but in few cases have any insights into the mechanism been elucidated (36). It is striking that the hepatitis B virus X protein (Hbx) has been suggested to interfere with the activity of the mitochondrial permeability pore, thus generating ROS with effects not unlike those we see in leporipoxvirus infections (52). In particular, this ROS has also been proposed to activate transcriptomes regulated by NF-κB and STAT-3 transcription factors and which, in cells constitutively expressing Hbx, might account for some of the pathological features of hepatocellular carcinomas (26).

In conclusion, the information that we have gathered from the study of leporipoxvirus SOD1 homologs led to the discovery of a novel poxvirus immunoevasion pathway that promotes virus-induced tumorigenesis. We suggest that these viral SOD1 homologs promote an increase in the levels of intracellular superoxide, which both stimulates cellular proliferation and inhibits apoptosis. Future work will focus on resolving where this ROS stress might be exerting its effect(s) on a complex chain of interlinked signal transduction cascades.

ACKNOWLEDGMENTS

We thank D. Benn and the staff and veterinarians at the Ontario Veterinary College for their help and assistance with animal studies. We also thank M. Barry, C. Bleackley, and S. Wasilenko (University of Alberta) for their help, gift of reagents, and advice with apoptotic measurements.

Operating and equipment grants provided to D.H.E. by the AHFMR, NSERC, and CIHR funded this work. M.T. is a recipient of an AHFMR graduate scholarship.

REFERENCES

1. **Almazan, F., D. C. Tscharke, and G. L. Smith.** 2001. The vaccinia virus superoxide dismutase-like protein (A45R) is a virion component that is nonessential for virus replication. J. Virol. **75:**7018–7029.
2. **Becker, M. N., W. B. Greenleaf, D. A. Ostrov, and R. W. Moyer.** 2004. *Amsacta moorei* entomopoxvirus expresses an active superoxide dismutase. J. Virol. **78:**10265–10275.
3. **Behrend, L., G. Henderson, and R. M. Zwacka.** 2003. Reactive oxygen species in oncogenic transformation. Biochem. Soc. Trans. **31:**1441–1444.
4. **Benhar, M., D. Engelberg, and A. Levitzki.** 2002. ROS, stress-activated kinases and stress signaling in cancer. EMBO Rep. **3:**420–425.
5. **Bennett, C. J., M. Webb, D. O. Willer, and D. H. Evans.** 2003. Genetic and phylogenetic characterization of the type II cyclobutane pyrimidine dimer photolyases encoded by leporipoxviruses. Virology **315:**10–19.
6. **Bize, I. B., L. W. Oberley, and H. P. Morris.** 1980. Superoxide dismutase and superoxide radical in Morris hepatomas. Cancer Res. **40:**3686–3693.
7. **Buttke, T. M., and P. A. Sandstrom.** 1994. Oxidative stress as a mediator of apoptosis. Immunol. Today **15:**7–10.
8. **Cameron, C., S. Hota-Mitchell, L. Chen, J. Barrett, J. X. Cao, C. Macaulay, D. Willer, D. Evans, and G. McFadden.** 1999. The complete DNA sequence of myxoma virus. Virology **264:**298–318.
9. **Cao, J. X., M. L. Teoh, M. Moon, G. McFadden, and D. H. Evans.** 2002. Leporipoxvirus Cu-Zn superoxide dismutase homologs inhibit cellular superoxide dismutase, but are not essential for virus replication or virulence. Virology **296:**125–135.
10. **Clement, M. V., and S. Pervaiz.** 1999. Reactive oxygen intermediates regulate cellular response to apoptotic stimuli: an hypothesis. Free Radic. Res. **30:**247–252.
11. **Clement, M. V., and I. Stamenkovic.** 1996. Superoxide anion is a natural inhibitor of FAS-mediated cell death. EMBO J. **15:**216–225.
12. **Culotta, V. C., L. W. Klomp, J. Strain, R. L. Casareno, B. Krems, and J. D. Gitlin.** 1997. The copper chaperone for superoxide dismutase. J. Biol. Chem. **272:**23469–23472.
13. **Everett, H., M. Barry, X. Sun, S. F. Lee, C. Frantz, L. G. Berthiaume, G. McFadden, and R. C. Bleackley.** 2002. The myxoma poxvirus protein, M11L, prevents apoptosis by direct interaction with the mitochondrial permeability transition pore. J. Exp. Med. **196:**1127–1139.
14. **Frank, S., H. Kampfer, M. Podda, R. Kaufmann, and J. Pfeilschifter.** 2000. Identification of copper/zinc superoxide dismutase as a nitric oxide-regulated gene in human (HaCaT) keratinocytes: implications for keratinocyte proliferation. Biochem. J. **346:**719–728.
15. **Fridovich, I.** 1978. The biology of oxygen radicals. Science **201:**875–880.
16. **Fridovich, I.** 1997. Superoxide anion radical ($O2^{\cdot-}$), superoxide dismutases, and related matters. J. Biol. Chem. **272:**18515–18517.
17. **Fujioka, S., J. Niu, C. Schmidt, G. M. Sclabas, B. Peng, T. Uwagawa, Z. Li, D. B. Evans, J. L. Abbruzzese, and P. J. Chiao.** 2004. NF-κB and AP-1 connection: mechanism of NF-κB-dependent regulation of AP-1 activity. Mol. Cell. Biol. **24:**7806–7819.
18. **Galeotti, T., H. Wohlrab, S. Borrello, and M. E. De Leo.** 1989. Messenger RNA for manganese and copper-zinc superoxide dismutases in hepatomas: correlation with degree of differentiation. Biochem. Biophys. Res. Commun. **165:**581–589.
19. **Gardner, P. R., and I. Fridovich.** 1992. Inactivation-reactivation of aconitase in Escherichia coli. A sensitive measure of superoxide radical. J. Biol. Chem. **267:**8757–8763.
20. **Gardner, P. R., I. Raineri, L. B. Epstein, and C. W. White.** 1995. Superoxide radical and iron modulate aconitase activity in mammalian cells. J. Biol. Chem. **270:**13399–13405.
21. **Halliwell, B., and J. M. C. Gutteridge.** 1999. Free radicals in biology and medicine, 3rd ed. Oxford University Press, New York, N.Y.
22. **Hernandez-Saavedra, D., and J. M. McCord.** 2003. Paradoxical effects of thiol reagents on Jurkat cells and a new thiol-sensitive mutant form of human mitochondrial superoxide dismutase. Cancer Res. **63:**159–163.
23. **Herrmann, M., H. M. Lorenz, R. Voll, M. Grunke, W. Woith, and J. R. Kalden.** 1994. A rapid and simple method for the isolation of apoptotic DNA fragments. Nucleic Acids Res. **22:**5506–5507.
24. **Kinnula, V. L., and J. D. Crapo.** 2004. Superoxide dismutases in malignant cells and human tumors. Free Radic. Biol. Med. **36:**718–744.
25. **Lamb, A. L., A. S. Torres, T. V. O'Halloran, and A. C. Rosenzweig.** 2001. Heterodimeric structure of superoxide dismutase in complex with its metallochaperone. Nat. Struct. Biol. **8:**751–755.
26. **Lee, Y. I., J. M. Hwang, J. H. Im, N. S. Kim, D. G. Kim, D. Y. Yu, H. B. Moon, and S. K. Park.** 2004. Human hepatitis B virus-X protein alters mitochondrial function and physiology in human liver cells. J. Biol. Chem. **279:**15460–15471.
27. **Malmstrom, B. G.** 1982. Enzymology of oxygen. Annu. Rev. Biochem. **51:**21–59.
28. **McCord, J. M.** 2000. The evolution of free radicals and oxidative stress. Am. J. Med. **108:**652–659.
29. **Opgenorth, A., N. Nation, K. Graham, and G. McFadden.** 1993. Transforming growth factor alpha, Shope fibroma growth factor, and vaccinia growth factor can replace myxoma growth factor in the induction of myxomatosis in rabbits. Virology **192:**701–709.
30. **Opgenorth, A., D. Strayer, C. Upton, and G. McFadden.** 1992. Deletion of the growth factor gene related to EGF and TGF alpha reduces virulence of malignant rabbit fibroma virus. Virology **186:**175–191.
31. **Parks, R. J., and D. H. Evans.** 1991. Effect of marker distance and orientation on recombinant formation in poxvirus-infected cells. J. Virol. **65:**1263–1272.
32. **Prose, P. H., A. E. Friedman-Kien, and J. Vilcek.** 1971. Morphogenesis of

rabbit fibroma virus. Correlation with pathogenesis of the skin lesion. Am. J. Pathol. **64:**467–478.
33. **Rojo, A. I., M. Salinas, D. Martin, R. Perona, and A. Cuadrado.** 2004. Regulation of Cu/Zn-superoxide dismutase expression via the phosphatidylinositol 3 kinase/Akt pathway and nuclear factor-κB. J. Neurosci. **24:**9324–9334.
34. **Rosen, D. R., T. Siddique, D. Patterson, D. A. Figlewicz, P. Sapp, A. Hentati, D. Donaldson, J. Goto, J. P. O'Regan, H. X. Deng, et al.** 1993. Mutations in Cu/Zn superoxide dismutase gene are associated with familial amyotrophic lateral sclerosis. Nature **362:**59–62.
35. **Schmidt, P. J., T. D. Rae, R. A. Pufahl, T. Hamma, J. Strain, T. V. O'Halloran, and V. C. Culotta.** 1999. Multiple protein domains contribute to the action of the copper chaperone for superoxide dismutase. J. Biol. Chem. **274:**23719–23725.
36. **Schwarz, K. B.** 1996. Oxidative stress during viral infection: a review. Free Radic. Biol. Med. **21:**641–649.
37. **Scott, C. B., R. Holdbrook, and S. Sell.** 1981. Cell-mediated immune response to Shope fibroma virus-induced tumors in adult rabbits. J. Natl. Cancer Inst. **66:**681–689.
38. **Seet, B. T., J. B. Johnston, C. R. Brunetti, J. W. Barrett, H. Everett, C. Cameron, J. Sypula, S. H. Nazarian, A. Lucas, and G. McFadden.** 2003. Poxviruses and immune evasion. Annu. Rev. Immunol. **21:**377–423.
39. **Senkevich, T. G., C. L. White, E. V. Koonin, and B. Moss.** 2002. Complete pathway for protein disulfide bond formation encoded by poxviruses. Proc. Natl. Acad. Sci. USA **99:**6667–6672.
40. **Shisler, J. L., T. G. Senkevich, M. J. Berry, and B. Moss.** 1998. Ultraviolet-induced cell death blocked by a selenoprotein from a human dermatotropic poxvirus. Science **279:**102–105.
41. **Shope, R. E.** 1932. A transmissible tumor-like condition of rabbits. J. Exp. Med. **56:**793–802.
42. **Smith, G. K., D. G. Barrett, K. Blackburn, M. Cory, W. S. Dallas, R. Davis, D. Hassler, R. McConnell, M. Moyer, and K. Weaver.** 2002. Expression, preparation, and high-throughput screening of caspase-8: discovery of redox-based and steroid diacid inhibition. Arch. Biochem. Biophys. **399:**195–205.
43. **Smith, G. L., Y. S. Chan, and S. T. Howard.** 1991. Nucleotide sequence of 42 kbp of vaccinia virus strain WR from near the right inverted terminal repeat. J. Gen. Virol. **72:**1349–1376.
44. **Smith, J. W., S. S. Tevethia, B. M. Levy, and W. E. Rawls.** 1973. Comparative studies on host responses to Shope fibroma virus in adult and newborn rabbits. J. Natl. Cancer Inst. **50:**1529–1539.
45. **Sun, Y., L. W. Oberley, T. D. Oberley, J. H. Elwell, and E. Sierra-Rivera.** 1993. Lowered antioxidant enzymes in spontaneously transformed embryonic mouse liver cells in culture. Carcinogenesis **14:**1457–1463.
46. **Sundaresan, M., Z. X. Yu, V. J. Ferrans, D. J. Sulciner, J. S. Gutkind, K. Irani, P. J. Goldschmidt-Clermont, and T. Finkel.** 1996. Regulation of reactive-oxygen-species generation in fibroblasts by Rac1. Biochem. J. **318:**379–382.
47. **Tanaka, M., K. Kogawa, Y. Nishihori, K. Kuribayashi, K. Nakamura, H. Muramatsu, K. Koike, S. Sakamaki, and Y. Niitsu.** 1997. Suppression of intracellular Cu-Zn SOD results in enhanced motility and metastasis of Meth A sarcoma cells. Int. J. Cancer **73:**187–192.
48. **Tarpey, M. M., and I. Fridovich.** 2001. Methods of detection of vascular reactive species: nitric oxide, superoxide, hydrogen peroxide, and peroxynitrite. Circ. Res. **89:**224–236.
49. **Teoh, M. L., P. J. Walasek, and D. H. Evans.** 2003. Leporipoxvirus Cu,Zn-superoxide dismutase (SOD) homologs are catalytically inert decoy proteins that bind copper chaperone for SOD. J. Biol. Chem. **278:**33175–33184.
50. **Vaquero, E. C., M. Edderkaoui, S. J. Pandol, I. Gukovsky, and A. S. Gukovskaya.** 2004. Reactive oxygen species produced by NAD(P)H oxidase inhibit apoptosis in pancreatic cancer cells. J. Biol. Chem. **279:**34643–34654.
51. **Wang, G., J. W. Barrett, S. H. Nazarian, H. Everett, X. Gao, C. Bleackley, K. Colwill, M. F. Moran, and G. McFadden.** 2004. Myxoma virus M11L prevents apoptosis through constitutive interaction with Bak. J. Virol. **78:**7097–7111.
52. **Waris, G., K. W. Huh, and A. Siddiqui.** 2001. Mitochondrially associated hepatitis B virus X protein constitutively activates transcription factors STAT-3 and NF-kappa B via oxidative stress. Mol. Cell. Biol. **21:**7721–7730.
53. **Wasilenko, S. T., A. F. Meyers, K. Vander Helm, and M. Barry.** 2001. Vaccinia virus infection disarms the mitochondrion-mediated pathway of the apoptotic cascade by modulating the permeability transition pore. J. Virol. **75:**11437–11448.
54. **Webb, M. A. M.** 2004. An investigation of factors affecting poxvirus genetic stability. National Library of Canada, Ottawa, Canada.
55. **Willer, D. O., G. McFadden, and D. H. Evans.** 1999. The complete genome sequence of Shope (rabbit) fibroma virus. Virology **264:**319–343.
56. **Willer, D. O., X. D. Yao, M. J. Mann, and D. H. Evans.** 2000. In vitro concatemer formation catalyzed by vaccinia virus DNA polymerase. Virology **278:**562–569.
57. **Zachertowska, A., D. Brewer, and D. H. Evans.** 2004. MALDI-TOF mass spectroscopy detects the capsid structural instabilities created by deleting the myxoma virus cupro-zinc SOD1 homolog M131R. J. Virol. Methods **122:**63–72.
58. **Zhang, Y., W. Zhao, H. J. Zhang, F. E. Domann, and L. W. Oberley.** 2002. Overexpression of copper zinc superoxide dismutase suppresses human glioma cell growth. Cancer Res. **62:**1205–1212.
59. **Zhao, H., S. Kalivendi, H. Zhang, J. Joseph, K. Nithipatikom, J. Vasquez-Vivar, and B. Kalyanaraman.** 2003. Superoxide reacts with hydroethidine but forms a fluorescent product that is distinctly different from ethidium: potential implications in intracellular fluorescence detection of superoxide. Free Radic. Biol. Med. **34:**1359–1368.